Effects of magnetic islands on drift wave instability

P. Jiang,[1,2,a)] Z. Lin,[2,b)] I. Holod,[2] and C. Xiao[1]
[1]*Fusion Simulation Center and State Key Laboratory of Nuclear Physics and Technology, Peking University, Beijing 100871, China*
[2]*Department of Physics and Astronomy, University of California, Irvine, California 92697, USA*

(Received 7 September 2014; accepted 28 November 2014; published online 12 December 2014)

Magnetic islands have been implemented in the gyrokinetic toroidal code to study the effects of the islands on microturbulence. The pressure profile flattening is verified in the simulation with the islands. Simulations of ion temperature gradient instability find that different toroidal modes are linearly coupled together and that toroidal spectra become broader when the island width increases. The real frequencies and growth rates of different toroidal modes approach each other with the averaged value independent of the island width. The linear mode structures are enhanced at the island separatrices and weakened at the island centers, consistent with the flattening of the pressure profile inside the islands. © *2014 AIP Publishing LLC*. [http://dx.doi.org/10.1063/1.4903910]

I. INTRODUCTION

The equilibrium magnetic field in toroidal plasmas (e.g., tokamak and stellarator) usually forms nested surfaces to confine charged particles. However, the topology of the magnetic surfaces can be destroyed by externally imposed perturbations such as the resonant magnetic perturbations[1] or by large-scale magnetohydrodynamic (MHD) instabilities such as tearing modes, which create magnetic islands. The magnetic field of the islands has a radial component, which can affect the neoclassical transport, microturbulence, and macroscopic MHD instabilities. For example, the plasma pressure flattening in the island region reduces the neoclassical bootstrap current, which leads to the growth of the island. This nonlinear tearing instability, neoclassical tearing mode (NTM), has been observed in many tokamak experiments.[2] The NTM can significantly limit the performance of high confinement tokamak operation and is a major concern for the ITER burning plasma.[3]

Meanwhile, the microturbulence regulates electron heat conductivity, which affects the pressure profile (and associated bootstrap current) in the island region. Furthermore, microturbulence can drive sheared flows by Reynolds stress and Maxwell stress, thus affecting the island dynamics. Therefore, fully self-consistent NTM simulation must incorporate nonlinear interaction between macroscopic MHD stability, neoclassical transport, and drift-Alfvenic microturbulence. Because the island evolution time is typically much longer than the time scale of microturbulence, static islands can be used to study the effects of the islands on the microturbulence and neoclassical transport.

The effects of static, mesoscale (low toroidal mode number) magnetic islands on microturbulence have recently been studied in nonlinear simulations.[4–8] Global particle and flux-tube continuum simulations of the ion temperature gradient (ITG) turbulence in the presence of the islands find that the ITG turbulence nonlinearly generates a long wavelength mode with the same toroidal mode number as the islands and an oscillating vortex mode with an electrostatic potential structure that coincides with the island topology.[5] The resulting vortex flows can suppress the microturbulence.[9] Finite pressure gradients inside the islands can be maintained by the turbulent transport[5] due to the turbulence spreading,[10] which allows finite bootstrap current inside the islands. Gyrokinetic continuum simulations of the ITG turbulence find that a nonambipolar radial current induces a torque to damp the toroidal rotation.[7] This microturbulence-induced torque also causes an oscillation of the islands as observed in the gyrofluid simulation of the ITG turbulence interaction with resistive tearing mode islands in the slab geometry.[8]

Despite the active research in the nonlinear effects on the microturbulence, the effects of the magnetic islands on the linear driftwave eigenmodes in the toroidal geometry have not been studied thoroughly. A gyrokinetic theory[11] finds that small magnetic islands in a sheared slab geometry can stabilize the ITG instability and modify the mode structure. However, the effects of the islands in toroidal geometry could be more complicated. For example, density and temperature profiles inside the island are mostly flattened on the inner mid-plane (i.e., high field side), but only partially flattened on the outer mid-plane (i.e., low field side) due to the toroidally trapped particles.[12] Moreover, electrons and ions respond differently to the islands due to their different orbit sizes and due to the island-trapped particles,[13] which induce two-dimensional electric fields inside and across the islands. Finally, the non-axisymmetric nature of the island perturbations could cause the linear coupling of different toroidal mode numbers.

In the current work, we use global gyrokinetic particle simulations to study the effects of the static magnetic islands on the linear eigenmodes of the ITG with adiabatic electrons. Magnetic islands with a single helicity are superimposed to a tokamak equilibrium with nested flux surfaces. Our simulations find that the island perturbations induce a linear coupling of the toroidal mode numbers and the coupling strength depends on the island sizes. The islands reduce the growth rate of the most unstable toroidal mode and enhance the growth rate of the subdominant toroidal modes. The frequency of the most unstable toroidal mode remains unchanged, while the frequencies of the subdominant toroidal modes approach the frequency of the most unstable

[a)]Electronic mail: jiangp@pku.edu.cn
[b)]Author to whom correspondence should be addressed. Electronic mail: zhihongl@uci.edu

modes when island size increases. The linear mode structures are enhanced at the island separatrices and weakened at the island centers, consistent with the flattening of the pressure profile inside the islands.

The current work utilizes the particle-in-cell gyrokinetic toroidal code (GTC),[14–16] which has been extensively applied to study turbulent transport in fusion plasmas including ion and electron temperature gradient modes,[17,18] collisionless trapped electron mode,[19] Alfvèn eigenmodes,[20,21] energetic particle transport,[22] and neoclassical transport.[23] The implementation of the equilibrium current[16] enables simulation of current-driven instability such as kink[24] and tearing modes.[25] Recently, three-dimensional (3D) equilibrium has been incorporated for simulations of stellarator and tokamak with 3D field. Magnetic island perturbations are implemented in the current work. These new GTC capabilities lay the foundations for the self-consistent simulation of NTM incorporating the interactions between magnetic islands, turbulent transport, and bootstrap current. As the first step, this paper reports electrostatic simulations of the island effects on the ITG with adiabatic electrons.

This paper is organized as follows. In Sec. II, we first describe the implementation of magnetic islands in the toroidal geometry. Then, we derive the gyrokinetic equations of motion with the static islands. In Sec. III, the island implementation is verified and the effects of static islands on the ITG are discussed. Finally, the conclusions are in Sec. IV.

II. FORMULATION AND IMPLEMENTATION OF MAGNETIC ISLANDS

A. Formulation of magnetic islands

In our simulations, the toroidal magnetic coordinate system (ψ, θ, ζ) is used, where ψ is the poloidal magnetic flux function, θ is the magnetic poloidal angle, and ζ is the magnetic toroidal angle. The covariant representation of the magnetic field[26] is

$$\mathbf{B}_0 = \delta\nabla\psi + I\nabla\theta + g\nabla\zeta, \tag{1}$$

the contravariant representation is

$$\mathbf{B}_0 = q\nabla\psi \times \nabla\theta - \nabla\psi \times \nabla\zeta, \tag{2}$$

and the Jacobian is

$$J^{-1} = \nabla\psi \cdot \nabla\theta \times \nabla\zeta = \frac{B_0^2}{gq + I}. \tag{3}$$

The radial component of the magnetic field $\delta\nabla\psi$ is small and usually neglected.[26] The island structure is introduced through a perturbed vector potential parallel to the background magnetic field,

$$\mathbf{A}_I = \alpha\mathbf{B}_0, \tag{4}$$

where $\alpha = \alpha_0(\psi)\cos(m\theta - n\zeta)$ for a single helicity. Multiple islands can be added straightforwardly. The magnetic field perturbation is

$$\delta\mathbf{B}_I = \nabla \times \alpha\mathbf{B}_0 = \frac{\partial\alpha}{\partial\psi} I\nabla\psi \times \nabla\theta + \frac{\partial\alpha}{\partial\psi} g\nabla\psi \times \nabla\zeta + \left(\frac{\partial\alpha}{\partial\zeta} I - \frac{\partial\alpha}{\partial\theta} g\right)\nabla\zeta \times \nabla\theta. \tag{5}$$

In this work, $\nabla \times \mathbf{B}_0 = 0$, i.e., we neglect the equilibrium current, which has previously been implemented in GTC simulation.[16] In the presence of this static magnetic island, the tokamak magnetic field can be represented as

$$\mathbf{B} = \mathbf{B}_0 + \delta\mathbf{B}_I = \left(q + \frac{\partial\alpha}{\partial\psi} I\right)\nabla\psi \times \nabla\theta - \left(1 - \frac{\partial\alpha}{\partial\psi} g\right)\nabla\psi \times \nabla\zeta + \left(\frac{\partial\alpha}{\partial\zeta} I - \frac{\partial\alpha}{\partial\theta} g\right)\nabla\zeta \times \nabla\theta. \tag{6}$$

Since $\delta\mathbf{B}_I \cdot \nabla\psi = \left(\frac{\partial\alpha}{\partial\theta} g - \frac{\partial\alpha}{\partial\zeta} I\right)\nabla\theta \times \nabla\zeta \cdot \nabla\psi \neq 0$, we need to find a new helical flux function[27] ψ_{he}, which satisfies $(\mathbf{B}_0 + \delta\mathbf{B}_I) \cdot \nabla\psi_{he} = 0$. The islands structures can be visualized by the contour plot of the helical flux function. Rewrite Eq. (6) as

$$\mathbf{B} = \left(q + \frac{\partial\alpha}{\partial\psi} I\right)\nabla\psi \times \nabla\xi - \left[\nabla\left(\psi - \frac{\psi_t}{q_s}\right) - \left(g + \frac{I}{q_s}\right)\nabla\alpha\right] \times \nabla\zeta, \tag{7}$$

where $\xi = \theta - \zeta/q_s$, q_s is the safety factor of the resonant surface and ψ_t is a toroidal flux function. Keeping terms up to the first order in r/R, the representation of the $\mathbf{B}$ field is

$$\mathbf{B} = q\nabla\psi \times \nabla\xi - \nabla\left(\psi - \frac{\psi_t}{q_s} - \alpha_0 g\cos m\xi\right) \times \nabla\zeta. \tag{8}$$

In order to satisfy the condition for a flux function, we choose the form of the helical flux as

$$\psi_{he} = \psi - \frac{\psi_t}{q_s} - \alpha_0 g\cos m\xi, \tag{9}$$

$$\mathbf{B} = q\nabla\psi \times \nabla\xi - \nabla\psi_{he} \times \nabla\zeta. \tag{10}$$

The radial island width W at $\theta = 0$ (defined as distance from island center to the last island surface) can be written as[5]

$$W = \sqrt{\frac{4R_0^2\alpha_0 q_s}{dq_s/dr}}, \tag{11}$$

where R_0 is the major radius and dq_s/dr is the gradient of the q profile at the resonant surface.

B. Gyrokinetic equations with static islands

We treat the static islands as the magnetic perturbation in the gyrokinetic equation. Using the gyrocenter position $\mathbf{X}$, magnetic moment μ, and the parallel velocity $v_\parallel$ as a set of independent variables, the gyrokinetic equation with island perturbations can be written as

$$\frac{d}{dt} f = \left[\frac{\partial}{\partial t} + \dot{\mathbf{X}} \cdot \nabla + \dot{v}_\parallel \frac{\partial}{\partial v_\parallel}\right] f = 0, \tag{12}$$

where

$$\dot{\mathbf{X}} = v_\parallel \frac{\mathbf{B}}{B_0} + \mathbf{v}_E + \mathbf{v}_d, \tag{13}$$

$$\dot{v}_\parallel = -\frac{1}{m}\frac{\mathbf{B}^*}{B_0}(\mu \nabla B_0 + Z_\sigma \nabla \phi), \tag{14}$$

where Z_σ is the particle charge, and m is the particle mass, $\mathbf{B}_0 = B_0 \mathbf{b}_0$ is the equilibrium magnetic field, $\mathbf{B} = \mathbf{B}_0 + \delta \mathbf{B}_I$, and

$$\mathbf{B}^* = \mathbf{B}_0^* + \delta \mathbf{B}_I = \mathbf{B}_0 + \frac{B_0 v_\parallel}{\Omega} \nabla \times \mathbf{b}_0 + \delta \mathbf{B}_I. \tag{15}$$

The $\mathbf{E} \times \mathbf{B}$ drift velocity is

$$\mathbf{v}_E = \frac{c \mathbf{b}_0 \times \nabla \phi}{B_0}, \tag{16}$$

and magnetic drift velocity is

$$\mathbf{v}_d = \mathbf{v}_c + \mathbf{v}_g, \tag{17}$$

where the magnetic curvature drift is

$$\mathbf{v}_c = \frac{v_\parallel^2}{\Omega} \nabla \times \mathbf{b}_0, \tag{18}$$

and the grad-B drift is

$$\mathbf{v}_g = \frac{\mu}{m\Omega} \mathbf{b}_0 \times \nabla B_0. \tag{19}$$

The electrostatic potential can be found using gyrokinetic Poisson equation, assuming a single ion species,

$$\frac{4\pi Z_i^2 n_i}{T_i}\left(\phi - \tilde{\phi}\right) = 4\pi (Z_i n_i - e n_e). \tag{20}$$

The density is defined as the fluid moments of the corresponding distribution functions,

$$n = \int f \, d\mathbf{v}, \tag{21}$$

where

$$\int d\mathbf{v} \equiv \frac{\pi B_0}{m} \int dv_\parallel d\mu. \tag{22}$$

The gyrokinetic equation (12) can be written as

$$Lf = 0, \tag{23}$$

where the propagator is separated into equilibrium (0th order), and perturbation parts $L = L_0 + \delta L$, with

$$L_0 = \frac{\partial}{\partial t} + \left(v_\parallel \mathbf{b}_0 + \mathbf{v}_d\right) \cdot \nabla - \frac{\mu}{m}\frac{\mathbf{B}_0^*}{B_0} \cdot \nabla B_0 \frac{\partial}{\partial v_\parallel} \tag{24}$$

and

$$\delta L = \left(v_\parallel \frac{\delta \mathbf{B}_I}{B_0} + \mathbf{v}_E\right) \cdot \nabla - \left(\mu \frac{\delta \mathbf{B}_I}{B_0} \cdot \nabla B_0 + Z \frac{\mathbf{B}^*}{B_0} \cdot \nabla \phi\right) \frac{1}{m} \frac{\partial}{\partial v_\parallel}. \tag{25}$$

The first term on the right hand side of Eq. (25) is the magnetic flutter term and is the dominant island contribution.

The distribution function can be decomposed into equilibrium and perturbed parts $f = f_0 + \delta f$. The equilibrium part satisfies the 0th order equation

$$L_0 f_0 = 0, \tag{26}$$

where f_0 is the neoclassical solution, approximated as a local Maxwellian in this work.

Subtracting Eq. (26) from Eq. (23), we get

$$L \delta f = -\delta L f_0. \tag{27}$$

Defining particle weight as $w = \frac{\delta f}{f}$, the nonlinear weight equation can be written as

$$\begin{aligned} Lw &= \frac{1}{f} L \delta f = -\frac{1}{f} \delta L f_0 = -\frac{f_0}{f}\left(\frac{1}{f_0} \delta L f_0\right) \\ &= -\frac{f - \delta f}{f}\left(\frac{1}{f_0} \delta L f_0\right) = -(1-w)\left(\frac{1}{f_0} \delta L f_0\right). \end{aligned} \tag{28}$$

In linear simulation, the weight is defined as $w = \frac{\delta f}{f_0}$ and the weight equation is reduced to

$$L_0 w = -\frac{1}{f_0} \delta L f_0. \tag{29}$$

The linear weight equation with island perturbation is

$$\begin{aligned} L_0 w = &-\left(v_\parallel \frac{\delta \mathbf{B}_I}{B_0} + \mathbf{v}_E\right) \cdot \frac{\nabla f_0}{f_0} \\ &+ \left(\mu \frac{\delta \mathbf{B}_I}{B_0} \cdot \nabla B_0 + Z \frac{\mathbf{B}^*}{B_0} \cdot \nabla \phi\right) \frac{1}{m f_0} \frac{\partial f_0}{\partial v_\parallel}. \end{aligned} \tag{30}$$

C. Implementation in Boozer coordinates

Assuming $\frac{\partial I}{\partial \psi} = 0$ and $\frac{\partial g}{\partial \psi} = 0$, the guiding center equations[26] with the island perturbation are

$$\dot{\zeta} = \frac{v_\parallel B_0 (q + I \partial_\psi \alpha)}{D} - c \frac{I}{D}\left[\frac{1}{Z}\frac{\partial \varepsilon}{\partial B_0}\frac{\partial B_0}{\partial \psi} + \frac{\partial \phi}{\partial \psi}\right], \tag{31}$$

$$\dot{\theta} = \frac{v_\parallel B_0 (1 - g \partial_\psi \alpha)}{D} + c \frac{g}{D}\left[\frac{1}{Z}\frac{\partial \varepsilon}{\partial B_0}\frac{\partial B_0}{\partial \psi} + \frac{\partial \phi}{\partial \psi}\right], \tag{32}$$

$$\begin{aligned} \dot{\psi} = &\frac{c}{Z}\frac{\partial \varepsilon}{\partial B_0}\left(\frac{I}{D}\frac{\partial B_0}{\partial \zeta} - \frac{g}{D}\frac{\partial B_0}{\partial \theta}\right) + \frac{cI}{D}\frac{\partial \phi}{\partial \zeta} - \frac{cg}{D}\frac{\partial \phi}{\partial \theta} \\ &+ v_\parallel B_0 \left(\frac{g}{D}\frac{\partial \alpha}{\partial \theta} - \frac{I}{D}\frac{\partial \alpha}{\partial \zeta}\right), \end{aligned} \tag{33}$$

$$\begin{aligned} \dot{\rho}_\parallel = &-c\frac{(1 - g\partial_\psi \alpha)}{D}\left[\frac{1}{Z}\frac{\partial \varepsilon}{\partial B_0}\frac{\partial B_0}{\partial \theta} + \frac{\partial \phi}{\partial \theta}\right] \\ &-c\frac{(q + I\partial_\psi \alpha)}{D}\left[\frac{1}{Z}\frac{\partial \varepsilon}{\partial B_0}\frac{\partial B_0}{\partial \zeta} + \frac{\partial \phi}{\partial \zeta}\right] \\ &+ c\frac{(I\partial_\zeta \alpha - g\partial_\theta \alpha)}{D}\left[\frac{1}{Z}\frac{\partial \varepsilon}{\partial B_0}\frac{\partial B_0}{\partial \psi} + \frac{\partial \phi}{\partial \psi}\right], \end{aligned} \tag{34}$$

where

$$\mathbf{B}_0 = \delta\nabla\psi + I\nabla\theta + g\nabla\zeta, \tag{35}$$

$$D = gq + I. \tag{36}$$

The modified parallel canonical momentum is

$$\rho_c = \rho_\parallel + \alpha, \tag{37}$$

with

$$\rho_\parallel = \frac{v_\parallel}{\Omega} = \frac{mc}{ZB_0} v_\parallel, \tag{38}$$

$$\alpha = \frac{A_{I\parallel}}{B_0}. \tag{39}$$

And we use

$$\frac{\partial \varepsilon}{\partial B_0} = \mu + \frac{Z^2}{mc^2}\rho_\parallel^2 B_0. \tag{40}$$

According to Eq. (30), the gyrokinetic equation for ions is

$$\frac{dw_i}{dt} = -\left(v_\parallel \frac{\delta\mathbf{B}_I}{B_0} + \mathbf{v}_E\right)\cdot\frac{\nabla f_{0i}}{f_{0i}} + \left(\mu\frac{\delta\mathbf{B}_I}{B_0}\cdot\nabla B_0 + Z_i\frac{\mathbf{B}^*}{B_0}\cdot\nabla\phi\right)\frac{1}{m_i f_{0i}}\frac{\partial f_{0i}}{\partial v_\parallel}. \tag{41}$$

It is more efficient to simulate tokamak in Boozer coordinates[26] (ψ, θ, ζ), where ψ is a poloidal magnetic flux function, θ is a poloidal angle, and ζ is a toroidal angle. The source terms in the right hand side of Eq. (41) need to be rewritten in Boozer coordinates. Assuming Maxwellian for the equilibrium distribution function in $(v_\parallel, v_\perp)$, the island perturbation terms on the RHS of Eq. (41) are

$$-v_\parallel\frac{\delta\mathbf{B}_I}{B_0}\cdot\frac{\nabla f_{0i}}{f_{0i}} + \mu\frac{\delta\mathbf{B}_I}{B_0}\cdot\nabla B_0\frac{1}{m_i}\frac{1}{f_{0i}}\frac{\partial f_{0i}}{\partial v_\parallel} = -v_\parallel\frac{\delta\mathbf{B}_I}{B_0}\cdot\left.\frac{\nabla f_{0i}}{f_{0i}}\right|_{v_\perp}. \tag{42}$$

The notation $\nabla f|_{v_\perp}$ represents derivative taken at $v_\perp = \text{const}$ instead of $\mu = \text{const}$. The $\mathbf{E}\times\mathbf{B}$ term on the RHS of Eq. (41) is

$$-\mathbf{v}_E\cdot\frac{\nabla f_{0i}}{f_{0i}} = -\frac{\mathbf{v}_E}{f_{0i}}\cdot\left[\nabla + \left(-\mu\frac{\nabla B_0}{B_0}\right)\left(-\frac{B_0}{T_i}\right)\right]f_{0i} + \mathbf{v}_E\cdot\frac{\mu\nabla B_0}{T_i} = -\frac{c\mathbf{b}_0\times\nabla\phi}{B_0}\frac{1}{f_{0i}}\cdot\left.\frac{\nabla f_{0i}}{f_{0i}}\right|_{v_\perp} - \frac{Z_i}{T_i}\mathbf{v}_g\cdot\nabla\phi. \tag{43}$$

The $\mathbf{B}^*$ term on the RHS of Eq. (41) is

$$Z_i\frac{\mathbf{B}^*}{B_0}\cdot\nabla\phi\frac{1}{m_i f_{0i}}\frac{\partial f_{0i}}{\partial v_\parallel} = Z_i\left(\mathbf{b}_0 + \frac{\delta\mathbf{B}_I}{B_0} + \frac{v_\parallel}{\Omega_i}\nabla\times\mathbf{b}_0\right)\nabla\phi\frac{1}{m_i f_{0i}}\frac{m_i v_\parallel}{-T_i}f_{0i} = -\frac{Z_i}{T_i}v_\parallel\left(\mathbf{b}_0 + \frac{\delta\mathbf{B}_I}{B_0}\right)\nabla\phi - \frac{Z_i}{T_i}\mathbf{v}_c\cdot\nabla\phi. \tag{44}$$

So, the gyrokinetic equation for ions with the island perturbation can be written as

$$\frac{dw_i}{dt} = -\left(\frac{c}{B_0}\mathbf{b}_0\times\nabla\phi + v_\parallel\frac{\delta\mathbf{B}_I}{B_0}\right)\cdot\left.\frac{\nabla f_{0i}}{f_{0i}}\right|_{v_\perp} - \frac{Z_i}{T_i}\left[v_\parallel\left(\mathbf{b}_0 + \frac{\delta\mathbf{B}_I}{B_0}\right) + \mathbf{v}_d\right]\cdot\nabla\phi. \tag{45}$$

The form of Eq. (45) (instead of Eq. (41)) is convenient for equilibrium Maxwellian distribution function in $(v_\parallel, v_\perp)$. Equation (45) can now be cast in Boozer coordinates. Assuming only radial dependence of the background density and temperature, the first term on the RHS of Eq. (45) is

$$-\frac{c}{B_0}\mathbf{b}_0\times\nabla\phi\cdot\left.\frac{\nabla f_{0i}}{f_{0i}}\right|_{v_\perp} = -\frac{c}{B_0^2 J}\left(I\frac{\partial\phi}{\partial\zeta} - g\frac{\partial\phi}{\partial\theta}\right)\frac{1}{f_{0i}}\left.\frac{\partial f_{0i}}{\partial\psi}\right|_{v_\perp}. \tag{46}$$

The third term on the RHS of Eq. (45) is

$$-\frac{Z_i}{T_i}v_\parallel\mathbf{b}_0\cdot\nabla\phi = -\frac{Z_i}{T_i}v_\parallel\frac{1}{B_0 J}\left(\frac{\partial\phi}{\partial\theta} + q\frac{\partial\phi}{\partial\zeta}\right). \tag{47}$$

The fourth term on the RHS of Eq. (45) is

$$-\frac{Z_i}{T_i}\mathbf{v}_d\cdot\nabla\phi = -\frac{Z_i}{T_i}\left(\frac{m_i v_\parallel^2}{B_0} + \mu\right)\frac{1}{Z_i}\frac{c}{B_0^2}\mathbf{B}_0\times\nabla\mathbf{B}_0\cdot\nabla\phi = -\frac{1}{T_i}\frac{c}{B_0^2 J}\left(\frac{m_i v_\parallel^2}{B_0} + \mu\right)\times\left(g\frac{\partial B_0}{\partial\psi}\frac{\partial\phi}{\partial\theta} - I\frac{\partial B_0}{\partial\psi}\frac{\partial\phi}{\partial\zeta} - g\frac{\partial B_0}{\partial\theta}\frac{\partial\phi}{\partial\psi}\right). \tag{48}$$

Since the radial component of the island magnetic field accounts for the most important modification of particle orbits, we consider $\frac{\partial\alpha}{\partial\psi} = 0$ for simplicity, which means the helical flux perturbation is independent of ψ. So, the source term of island perturbation on the RHS of Eq. (45) is

$$-v_\parallel\frac{\delta\mathbf{B}_I}{B_0}\cdot\left.\frac{\nabla f_{0i}}{f_{0i}}\right|_{v_\perp} - \frac{Z_i}{T_i}v_\parallel\frac{\delta\mathbf{B}_I}{B_0}\cdot\nabla\phi = \frac{v_\parallel}{B_0 J}\left(\frac{\partial\alpha}{\partial\zeta}I - \frac{\partial\alpha}{\partial\theta}g\right)\left[\frac{1}{f_{0i}}\left.\frac{\partial f_{0i}}{\partial\psi}\right|_{v_\perp} + \frac{Z_i}{T_i}\frac{\partial\phi}{\partial\psi}\right]. \tag{49}$$

Finally, the linear gyrokinetic equation (45) in Boozer coordinates can be rewritten as

$$\frac{dw_i}{dt} = -\frac{c}{B_0^2 J}\left(I\frac{\partial\phi}{\partial\zeta} - g\frac{\partial\phi}{\partial\theta}\right)\frac{1}{f_{0i}}\left.\frac{\partial f_{0i}}{\partial\psi}\right|_{v_\perp} - \frac{Z_i}{T_i}v_\parallel\times\frac{1}{B_0 J}\left(\frac{\partial\phi}{\partial\theta} + q\frac{\partial\phi}{\partial\zeta}\right) - \frac{1}{T_i}\frac{c}{B_0^2 J}\left(\frac{m_i v_\parallel^2}{B_0} + \mu\right)\times\left(g\frac{\partial B_0}{\partial\psi}\frac{\partial\phi}{\partial\theta} - I\frac{\partial B_0}{\partial\psi}\frac{\partial\phi}{\partial\zeta} - g\frac{\partial B_0}{\partial\theta}\frac{\partial\phi}{\partial\psi}\right) + \frac{v_\parallel}{B_0 J}\left(\frac{\partial\alpha}{\partial\zeta}I - \frac{\partial\alpha}{\partial\theta}g\right)\left[\frac{1}{f_{0i}}\left.\frac{\partial f_{0i}}{\partial\psi}\right|_{v_\perp} + \frac{Z_i}{T_i}\frac{\partial\phi}{\partial\psi}\right]. \tag{50}$$

III. SIMULATION OF ITG IN THE PRESENCE OF STATIC ISLANDS

A. Verification of island implementation

There are two steps to verify the implementation of magnetic islands in the GTC code. We first create the contour plot of helical flux to demonstrate the island structure. Since the particles move along the perturbed field lines, the density and temperature profiles inside the island region become flattened after several transit times. We then verify the island implementation by demonstrating that the density profile is flattened inside the island region for simulation with uniform temperature.

Since the equilibrium poloidal flux surfaces are no longer valid, the helical flux function is used to describe the island structures. Fig. 1 is the contour plot of the helical flux at $\zeta = 0$ for the islands described by a perturbed vector potential $A_{I\|} = -0.0001 R_0 B_0 \cos(m\theta - n\zeta)$. The closed lines represent the helical flux surfaces. The inverse aspect ratio is $a/R_0 = 0.42$, where R_0 and a are the tokamak major and minor radii. The island width is $w = 0.16a$ and the island helicity is m = 2, n = 1. We will use these islands in the following simulations. In the contour plot, the two islands have different sizes at the high field and low field sides because the Jacobians are different.

The density and temperature profile can be flattened inside the islands due to the parallel motion of the particles. In the simulation, we use uniform temperature and $R_0/L_{ni} = 1.9$, where $L_{ni} = \frac{n_i}{dn_i/dr}$ is the initial ion density scale length at the center of islands. Because $a/\rho_i = 150$ and $w/\rho_i = 24$, the finite-Lamor-radius effect is not significant. By excluding the self-consistent electric field and collisions, the only perturbation is the magnetic islands. In this regime, ions can move along the perturbed field lines in the presence of magnetic islands. So the ion density profile inside the island should be flattened. In Fig. 2, the ion density gradient at the island center at the high-field side decreases to zero after about 19 ion transit times ($120\, R_0/c_s$) and slightly oscillate around zero after that.

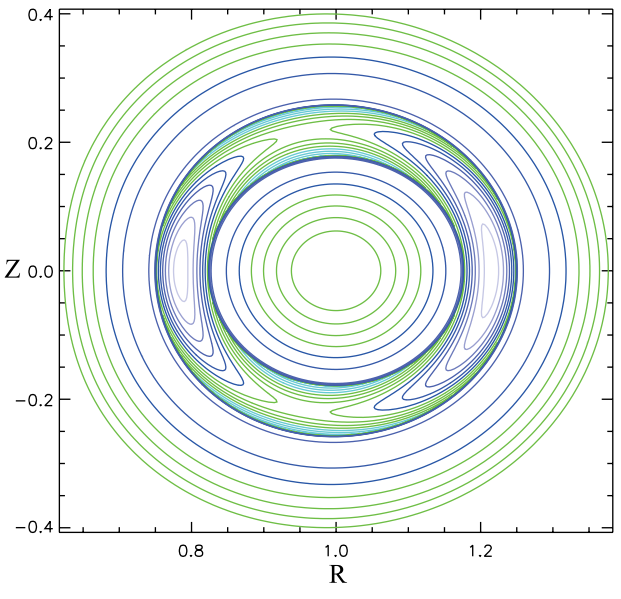

FIG. 1. Helical flux surfaces of (2, 1) islands in the $\zeta = 0$ poloidal plane.

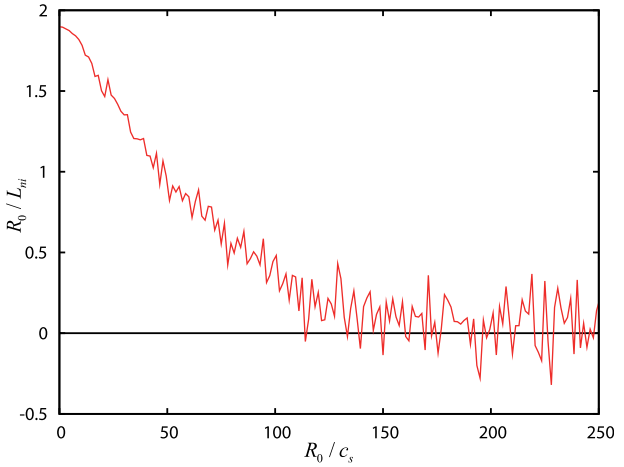

FIG. 2. Time history of ion density gradient at the island center at the high field side.

After the ion density gradient at the island center becomes zero, we perform a time average of the radial ion density profile at $\theta = 0, \pi$ from time $t = 120 R_0/c_s$ to 250 R_0/c_s. In Fig. 3, the vertical lines are the island separatrix. The density profile at the low field side (black dashed line) is less flattened than that at the high field side (green dotted line) because there are more toroidally trapped ions in the low field side, which do not move along the perturbed magnetic field lines. Unlike the passing ions which can move from one side to the other side across the island regions, the deeply trapped ions only bounce at one side of the island. This bounce motion of the toroidally trapped ions prevents the flattening of the equilibrium density profile at the island center.

In order to get an intuitive picture of the density distribution across the islands, we plot this density averaged over the period $t = 120$–$250 R_0/c_s$ in the poloidal plane at $\zeta = 0$ in Fig. 4. The black lines in Figure 4 are the helical flux surfaces. The ion density inside the island region is almost

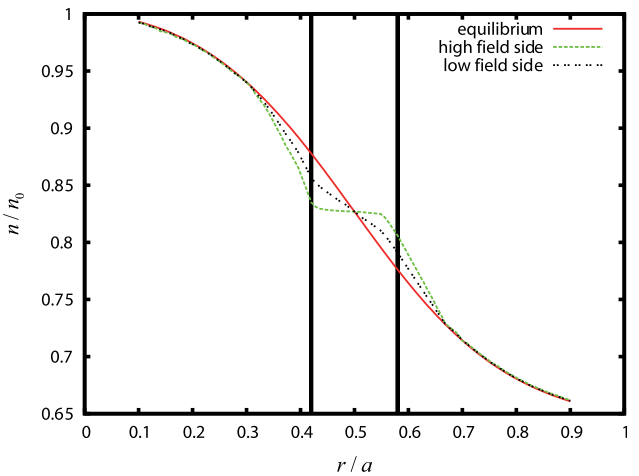

FIG. 3. Radial profile of ion density at $\theta = 0, \pi$. The red solid line is equilibrium ion density profile. The green dotted line is the ion density profile in the high field side ($\theta = \pi$). The black dashed line is the ion density profile in the low field side ($\theta = 0$).

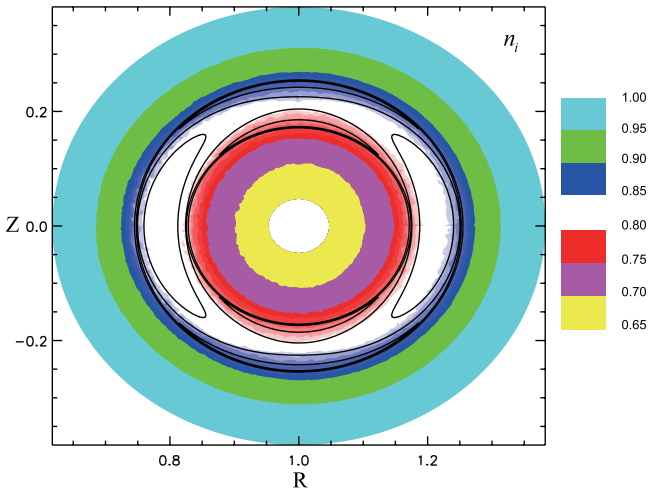

FIG. 4. Poloidal snapshot of ion density with islands.

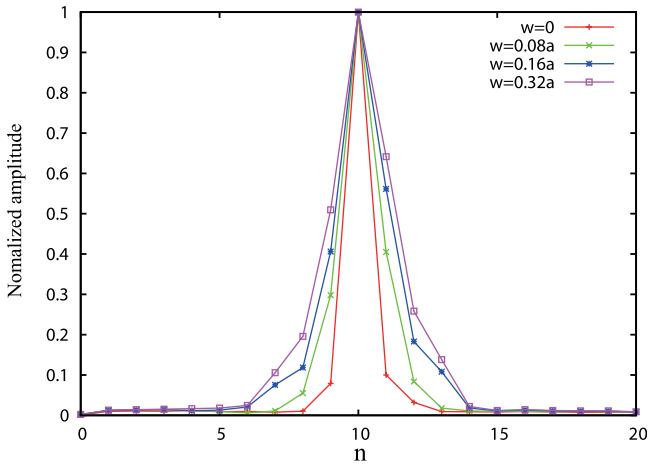

FIG. 5. Toroidal mode spectrum from four simulation cases with different island sizes.

uniform, while finite density gradient exists near the island boundary.

In conclusion, the density profile becomes partially flattened across the islands (shown in Figs. 3 and 4). Instead of setting the density profile artificially flat, our simulation allows the system to evolve self-consistently to the steady state induced by the island perturbation. A more systematic study of the equilibrium density profiles in the presence of the magnetic islands including the effects of collisions will appear in another paper.[13] Our next simulation about effects of static islands on the ITG instability will start at this new equilibrium state, in which the density profile is partially flattened across the islands region.

B. Effects of static islands on ITG

After verification of the island implementation, we use GTC to study the effects of magnetic islands on the ITG instability. The pressure gradient is maximal at the radial position $r/a = 0.5$. The parameters for the background plasma are $R_0/L_{Ti} = R_0/L_{Te} = 6.0$, $R_0/L_{ni} = R_0/L_{ne} = 1.9$ at $r/a = 0.5$, and $T_e = T_i$. Electrons are adiabatic. Diagnostic is taken at the radial position $r/a = 0.5$, where $q = 2$ and $\hat{s} = 0.38$. We start the simulation without turbulence and only keep the island effects. When the system reaches the new equilibrium in Fig. 3, in which the ion density profile is flattened inside the islands, we turn on the turbulence to study the effects of static islands on ITG.

We investigate the toroidal modes spectrum to clarify the linear coupling of different toroidal modes induced by the islands. In the linear simulation keeping all the toroidal modes, we measure the mode amplitudes with different toroidal numbers and normalize these toroidal modes amplitudes such that the maximal mode amplitude is unity. Fig. 5 shows the toroidal modes spectrum from four simulations with different island widths. The red line represents the toroidal mode spectrum without islands, where there is only one dominant mode with n = 10 or $k_\theta \rho_i = 0.267$. In the case of $W = 0.16a$, the toroidal mode spectrum becomes broader due to the toroidal mode coupling by the islands. When we decrease the island width by half ($W = 0.08a$), the spectrum becomes narrower but still broader than that without islands. As we increase the island width ($W = 0.32a$), the spectrum becomes even broader than that with ($W = 0.16a$) islands. In conclusion, the islands can induce toroidal mode coupling. When we increase the island width, this coupling becomes stronger, which leads to a wider toroidal mode spectrum.

Furthermore, the islands can cause frequencies and growth rates of different toroidal modes to couple together. Here, we use n = 9 and m = 18, n = 10 and m = 20, n = 11 and m = 22 harmonics to measure the real frequency and growth rate. In Fig. 6(a), the growth rates of these three modes approach the same value as the island width increases. The average of the growth rates of these three modes is 0.281, which is independent of the island widths. In Fig. 6(b), the real frequencies of n = 9, 10, 11 modes

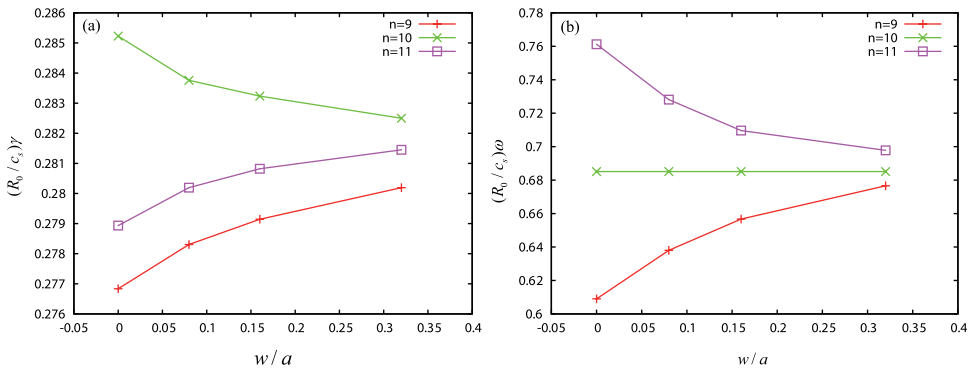

FIG. 6. Growth rate (a) and real frequency (b) of different toroidal modes from four simulations with different island sizes.

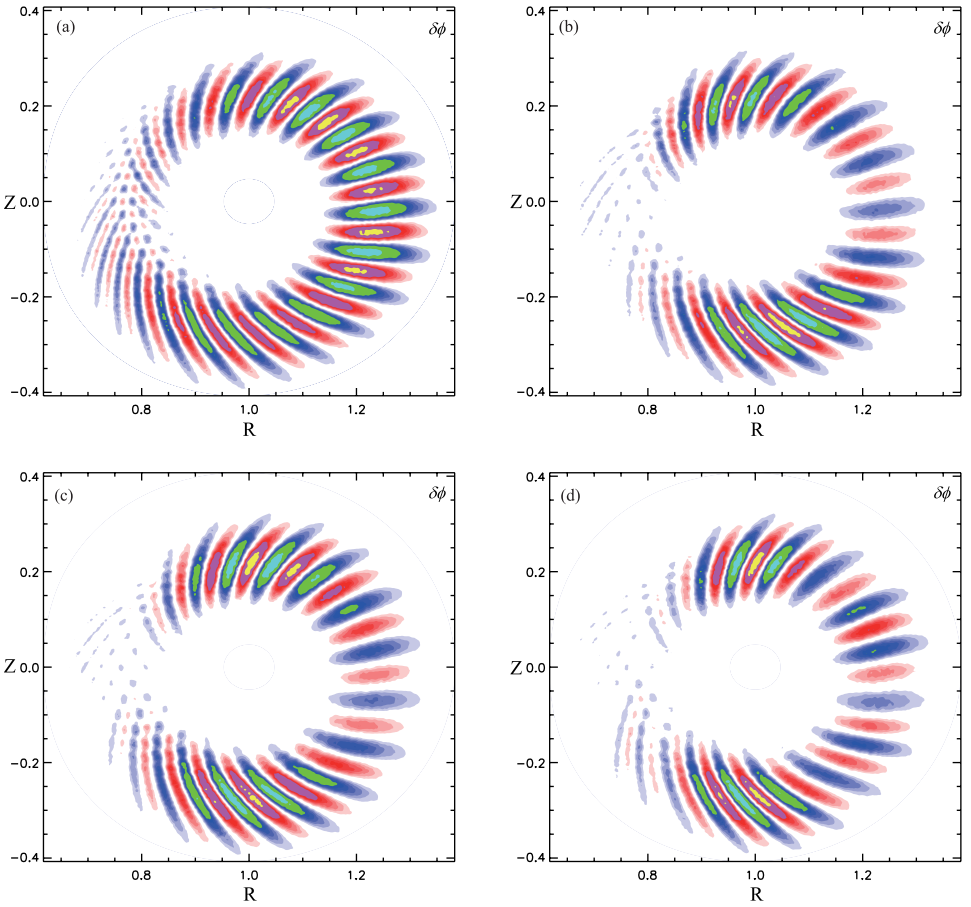

FIG. 7. Poloidal snapshot of electrostatic potential without islands (panel (a)) and with W = 0.16a islands at different times (panels (b), (c), and (d)).

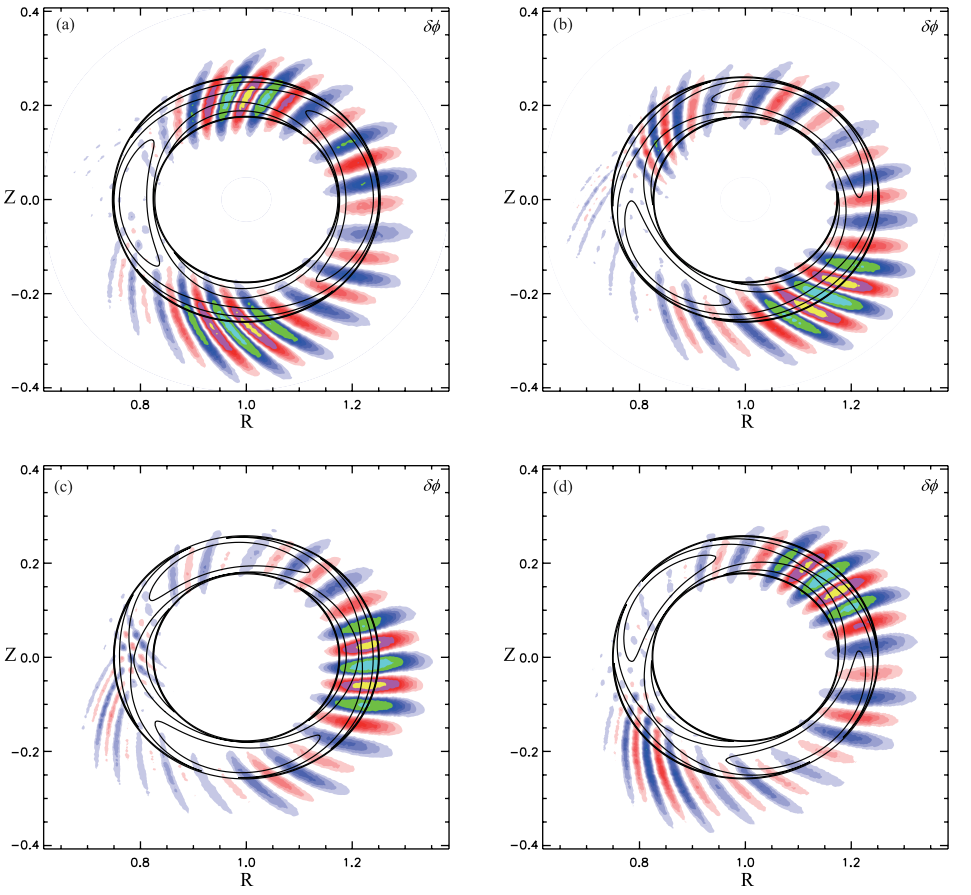

FIG. 8. Poloidal snapshot of electrostatic potential with W = 0.16a islands at different toroidal angles $\zeta = 0, \frac{\pi}{2}, \pi, \frac{3\pi}{2}$ (panels (a), (b), (c), (d)).

approach that of the n = 10 mode as the island width increases. The average of the real frequency of these three modes is 0.682, which is independent of the island widths. Our simulation results show that the island-induced coupling is not complete as different toroidal modes maintain slightly different real frequencies and growth rates.

In Fig. 7(a), snapshot of the electrostatic potential in the $\zeta = 0$ poloidal plane shows good ballooning mode structure with the dominant poloidal number $m = 20$ in the absence of the islands. But when we include the island perturbation, the mode structure is changed due to the toroidal mode coupling. The mode structures are results of linear superposition of different toroidal mode numbers (dominated by n = 9, 10, 11). The poloidal mode structure at an early phase of the exponential growth (defined as time t = 0) is shown in Fig. 7(b). The electrostatic potential is enhanced at $\theta = \frac{\pi}{2}, \frac{3\pi}{2}$ (i.e., island separatrices) and weakened at $\theta = 0, \pi$ (i.e., island centers). The mode structures at later times $\gamma t = 11.3$ and $\gamma t = 22.6$ are shown in Figs. 7(c) and 7(d), respectively. The mode structure rotates very slowly due to the slightly different real frequencies of the three dominant toroidal mode numbers (n = 9, 10, 11). In fact, the mode structure changes are very insignificant over a period of 22.6 linear growth times (from Figs. 7(b) to 7(d)). The linear growth time is a relevant time scale since the linear mode structure will be destroyed over a period of the linear growth time by nonlinear effects in the nonlinear simulation.

Fig. 8 shows poloidal contour plots of ITG mode structure at four toroidal locations $\zeta = 0, \frac{\pi}{2}, \pi, \frac{3\pi}{2}$ at the same time of panel (d) in Fig. 7. ITG is always suppressed in the island center, which moves to different poloidal angles at different toroidal angles. Therefore, both Figs. 7 and 8 show that linear ITG mode structures are enhanced at the island separatrices and weakened at the island centers, consistent with the flattening of the pressure profile inside the islands as shown in Fig. 4.

IV. SUMMARY

In this work, we have implemented magnetic islands in the GTC and studied the effects of magnetic islands on the ITG instability. The density profile flattening due to the islands is verified in the simulation, which only includes island fields. In the ITG simulations, the ITG toroidal modes spectrum becomes broader when island width increases. The real frequencies and growth rates of different modes tend to couple together. Due to the coupling between different toroidal modes, several modes structures with different toroidal numbers are superimposed to form the new mode structure. The linear mode structures are enhanced at the island separatrices and weakened at the island centers, consistent with the flattening of the pressure profile inside the islands. In the next step, the drift-kinetic electrons will be included in the non-linear simulation of islands and microturbulence to study the effects of islands on the zonal flows.

ACKNOWLEDGMENTS

The authors are grateful for the discussions with and support of the GTC team. This work was supported by China National Magnetic Confinement Fusion Science Program (Grants No. 2013GB111000 and No. 2014GB107004), China Scholarship Council (Grant 2011601098), U.S. DOE Grants DE-SC0010416 and DE-FG02-07ER54916. This research used resources of the Oak Ridge Leadership Computing Facility at Oak Ridge National Laboratory (DOE Contract No. DE-AC05-00OR22725), and the National Energy Research Scientific Computing Center (DOE Contract No. DE-AC02-05CH11231).

[1]T. E. Evans, M. E. Fenstermacher, R. A. Moyer, T. H. Osborne, J. G. Watkins, P. Gohil, I. Joseph, M. J. Schaffer, L. R. Baylor, M. Becoulet *et al.*, Nucl. Fusion **48**, 024002 (2008).
[2]Z. Chang, J. D. Callen, E. D. Fredrickson, R. V. Budny, C. C. Hegna, K. M. McGuire, M. C. Zarnstorff, and TFTR group, Phys. Rev. Lett. **74**, 4663 (1995).
[3]T. C. Hender, J. C. Wesley, J. Bialek, A. Bondeson, A. H. Boozer, R. J. Buttery, A. Garofalo, T. P. Goodman, R. S. Granetz, Y. Gribov *et al.*, Nucl. Fusion **47**, S128 (2007).
[4]E. Poli, A. Bottino, and A. G. Peeters, Nucl. Fusion **49**, 075010 (2009).
[5]E. Poli, A. Bottino, W. A. Hornsby, A. G. Peeters, T. Ribeiro, B. D. Scott, and M. Siccinio, Plasma Phys. Controlled Fusion **52**, 124021 (2010).
[6]W. A. Hornsby, A. G. Peeters, A. P. Snodin, F. J. Casson, Y. Camenen, G. Szepesi, M. Siccinio, and E. Poli, Phys. Plasmas **17**, 092301 (2010).
[7]R. E. Waltz and F. L. Waelbroeck, Phys. Plasmas **19**, 032508 (2012).
[8]J. Li and Y. Kishimoto, Phys. Plasmas **19**, 030705 (2012).
[9]Z. X. Wang, J. Q. Li, J. Q. Dong, and Y. Kishimoto, Phys. Rev. Lett. **103**, 015004 (2009).
[10]Z. Lin and T. S. Hahm, Phys. Plasmas **11**, 1099 (2004).
[11]H. R. Wilson and J. W. Connor, Plasma Phys. Controlled Fusion **51**, 115007 (2009).
[12]W. A. Hornsby, M. Siccinio, A. G. Peeters, E. Poli, A. P. Snodin, F. J. Casson, Y. Camenen, and G. Szepesl, Plasma Phys. Controlled Fusion **53**, 054008 (2011).
[13]G. Dong, Z. Lin, and P. Jiang, "Effects of magnetic islands on neoclassical bootstrap current" (in preparation).
[14]Z. Lin, T. S. Hahm, W. W. Lee, W. M. Tang, and R. B. White, Science **281**, 1835 (1998).
[15]I. Holod, W. L. Zhang, Y. Xiao, and Z. Lin, Phys. Plasmas **16**, 122307 (2009).
[16]W. Deng, Z. Lin, and I. Holod, Nucl. Fusion **52**, 023005 (2012).
[17]Z. Lin, I. Holod, L. Chen, P. H. Diamond, T. S. Hahm, and S. Ethier, Phys. Rev. Lett. **99**, 265003 (2007).
[18]Z. H. Lin, S. Ethier, T. S. Hahm, and W. M. Tang, Plasma Sci. Technol. **14**, 1125 (2012).
[19]Y. Xiao and Z. Lin, Phys. Rev. Lett. **103**, 085004 (2009).
[20]H. S. Zhang, Z. Lin, and I. Holod, Phys. Rev. Lett. **109**, 025001 (2012).
[21]Z. Wang, Z. Lin, I. Holod, W. W. Heidbrink, B. Tobias, M. Van Zeeland, and M. E. Austin, Phys. Rev. Lett. **111**, 145003 (2013).
[22]W. Zhang, Z. Lin, and L. Chen, Phys. Rev. Lett. **101**, 095001 (2008).
[23]Z. Lin, W. M. Tang, and W. W. Lee, Phys. Rev. Lett. **78**, 456 (1997).
[24]J. McClenaghan, Z. Lin, I. Holod, and W. Deng, Phys. Plasmas (to be published).
[25]D. Liu, W. Zhang, J. McClenaghan, J. Wang, and Z. Lin, Phys. Plasmas (to be published).
[26]R. B. White and M. S. Chance, Phys. Fluids **27**, 2455 (1984).
[27]R. Carrera, R. D. Hazeltine, and M. Kotschenreuther, Phys. Fluids **29**, 899 (1986).